

# RSC Advances



This is an *Accepted Manuscript*, which has been through the Royal Society of Chemistry peer review process and has been accepted for publication.

*Accepted Manuscripts* are published online shortly after acceptance, before technical editing, formatting and proof reading. Using this free service, authors can make their results available to the community, in citable form, before we publish the edited article. This *Accepted Manuscript* will be replaced by the edited, formatted and paginated article as soon as this is available.

You can find more information about *Accepted Manuscripts* in the [Information for Authors](#).

Please note that technical editing may introduce minor changes to the text and/or graphics, which may alter content. The journal's standard [Terms & Conditions](#) and the [Ethical guidelines](#) still apply. In no event shall the Royal Society of Chemistry be held responsible for any errors or omissions in this *Accepted Manuscript* or any consequences arising from the use of any information it contains.

## Tailored graphene based polyurethane composites for efficient electrostatic dissipation and electromagnetic interference shielding applications

Meenakshi Verma<sup>1</sup>, Pawan Verma<sup>1</sup>, S K Dhawan<sup>2</sup>, Veena Choudhary<sup>1\*</sup>

<sup>1</sup> *Centre for Polymer Science & Engineering,*

*Indian Institute of Technology, Hauz Khas, New Delhi, 110016, India*

<sup>2</sup> *Polymeric & Soft Materials Section, National Physical Laboratory (CSIR)*

*Dr. K. S. Krishnan Road, New Delhi, 110 012, India*

*\*E-mail:veenach@hotmail.com*

### **Abstract**

Nanocomposite materials based on commercial thermoplastic polyurethane filled with graphene are new alternative candidates for electrostatic charge dissipation and electromagnetic interference shielding applications due to their lightweight, ease of processing and tunable electrical conductivities. Solution blending approach was used to fabricate a series of polyurethane/graphene (PUG) nanocomposites with graphene loading ranging from 0 – 5.5 vol. %. For the preparation of polymer nanocomposites, graphene was prepared by the successful oxidation of pristine graphite followed by thermal exfoliation and reduction. The effect of graphene on the electrical properties of PUG nanocomposites was investigated to evaluate the potential of these nanocomposites as an effective and light weight electrostatic charge dissipative (ESD) and electromagnetic interference (EMI) shielding material in the frequency range of 8.2-12.4 GHz (X band). The suitability of the nanocomposites for ESD was examined by displaying the decay of voltage as a function of time. The experimental results indicate that the static decay time of 0.49 sec at 1.6 vol. % graphene and EMI shielding effectiveness of ~ -21 dB in X-band for 3mm thickness was achieved at 5.5 vol. % graphene loading. In addition, the electromagnetic attributes such as real and imaginary permittivity of composites as a function of frequency were also investigated. Therefore, such polyurethane nanocomposites shall not only be useful for

antistatic coatings but also have great potential as an effective and light weight shielding materials for protection from electromagnetic radiation, in making electromagnetic shielding bags for packaging of electronic circuits and variety of applications.

## Introduction

Electrically conductive polymer composite (ECPC) materials have received tremendous attention for a variety of applications such as static charge dissipation and electromagnetic/radio frequency interference (EMI/RFI) shielding.<sup>1</sup> In recent years, industry has demanded a range of materials that not only possess strength, wear properties, heat and chemical resistance but materials that can prevent the build-up of a static charge and suppress or eliminate the EM radiations radiated by electronic instruments. Typically, materials such as metals, different forms of carbon, e.g., graphite and its exotic forms such as flexible graphite, expanded graphite, single or multiwalled carbon nanotubes, carbon fibers, carbon black, reduced graphene oxide (RGO), graphene, conducting polymers, dielectric, magnetic materials and their composites have been widely used as EMI shields due to their high conductivity and good dielectric and magnetic properties.<sup>2-4</sup> However, metals have disadvantages, such as heavy weight, corrosion susceptibility and cumbersome processing methods, which make these materials unsuitable for both the researchers and users. ECPC's features conductive fillers homogeneously dispersed in insulating polymer matrices commonly characterized by an insulator-conductor transition at certain critical conductive filler content, also known as percolation threshold.<sup>5</sup> Polymeric materials have been largely used as a matrix for developing EMI shields because of their easy fabrication into various shapes. Lightweight, corrosion resistance and flexibility are the important technical requirements for a high performance EMI shield for applications in aerospace, aircrafts, automobiles, flexible

electronics and wearable devices.<sup>6</sup> The EMI shielding efficiency of a composite material depends on the filler's intrinsic conductivity, dielectric constant and aspect ratio etc.<sup>7</sup>

Graphene, as promising conductive filler, has acquired tremendous consideration owing to its unique properties such as remarkable structural flexibility, superior electrical conductivity, thermal stability and excellent mechanical properties.<sup>8</sup> These extraordinary properties make graphene and graphene-like nanomaterials very promising candidates for many potential applications in many technological fields such as polymer nanocomposites,<sup>9</sup> supercapacitors,<sup>10-12</sup> nanoelectronics,<sup>13</sup> energy storage devices,<sup>14-16</sup> batteries<sup>17-21</sup> and sensors.<sup>22</sup> The excellent electrical properties and high specific surface area make graphene very promising for electromagnetic shields to absorb incident electromagnetic waves. In the drive to develop efficient microwave absorbers and electromagnetic shields, graphene and graphene based composites have received tremendous attention in recent years due to the rapid growth of electronic industry.<sup>23-26</sup> Graphene is highly desirable as an electromagnetic wave absorber at high frequencies over the gigahertz range due to its high dielectric loss and low density.<sup>27</sup>

Among the thermoplastic polymers, thermoplastic polyurethanes (TPU) have attracted a great deal of attention due to their combination of properties such as flexibility, stretchability, transparency, good abrasion and chemical resistance, good wear and weather resistance and good mechanical properties.<sup>28</sup> Polyurethanes are widely used in flexible displays,<sup>29</sup> smart clothing,<sup>30</sup> electronic textiles, durable elastomeric wheels and tires (such as roller coaster, escalator and skateboard wheels),<sup>31</sup> high performance adhesives, hard plastic parts (e.g. for electronic instruments) and surface coatings and sealants.<sup>32</sup> The scope of applications of TPU can be further increased by incorporating carbon based fillers into TPU which not only enhance the mechanical

properties but also develop conductivity in non-conducting matrix for newer applications such as ESD and EMI shielding materials.<sup>33-35</sup>

Several studies on microwave absorption and EMI shielding properties of polyurethane composites containing graphene have been discussed in the previous reports. Nanni et al reported an average value of -20 dB of shielding effectiveness in X band in case of TPU having 20 wt. % exfoliated graphite and 4 mm thick sample.<sup>36</sup> Yang et al studied the EMI shielding performance of polydopamine coated graphene nanosheets incorporated in polyurethane and obtained -17.6 dB at 1.2 GHz in the frequency range of 30MHz-1.8GHz with 4.75 vol. % loading.<sup>37</sup> Hsiao et al. fabricated electrospun water based polyurethane featuring sulfonate groups/HI reduced graphene by L-b-L assembly to achieve an EMI shielding effectiveness of -34 dB in the X-band for 1 mm thick sample.<sup>38</sup> In another course of investigation, Hsiao and his coworkers prepared water based polyurethane composites using non-covalently modified exfoliated graphene nanosheets and reported a maximum shielding effectiveness of -32 dB at 7.7 wt. % filler content in the frequency range of 8.2 - 12.4 GHz.<sup>39</sup> Composites of covalently modified graphene nanosheets dispersed in water based polyurethane matrix with grafted sulfonate functional groups exhibited an EMI shielding effectiveness of -38 dB over the frequency of 8.2 to 12.4 GHz.<sup>40</sup> In the above studies, it was observed that the high shielding effectiveness was achieved either at a very high filler content or the filler has been extensively modified using complicated reactions which will restrict their utilization and commercialization.

The aim of this paper is to study the effect of incorporation of thermally reduced graphene oxide (RGO) on the electrical properties of thermoplastic polyurethane (TPU) for ESD and EMI shielding applications. In this research, composite samples made of RGO (at varying loading) dispersed in TPU matrix were prepared and investigated for their potential as an effective and

light weight EMI shielding material in the frequency range of 8.2 - 12.4 GHz (X band). Unlike for most previously reported graphene based composite systems that suggest their usefulness for antistatic and electrostatic charge dissipation applications simply on the basis of electrical conductivity<sup>41-43</sup>, the antistatic decay time was measured for the first time quantitatively.

### **Materials**

Commercially available thermoplastic polyurethane (TPU, Desmopan) was purchased from Bayer Material Science, India. Natural graphite powder (300 mesh size) was purchased from Loba Chemie, India. Concentrated sulphuric acid (H<sub>2</sub>SO<sub>4</sub>, 98%), ortho-phosphoric acid (o-H<sub>3</sub>PO<sub>4</sub>, 88%), hydrochloric acid (HCl, 37%) hydrogen peroxide (H<sub>2</sub>O<sub>2</sub>, 50%), N, N-dimethyl formamide (DMF, 99.5% GR) all from Merck, Belgium, potassium permanganate (KMnO<sub>4</sub>) and ethanol (Fischer Scientific, India) were used as received without further purification.

### **Synthesis of GO and RGO**

GO was synthesized from natural graphite powder using an improved Hummers method according to the procedure provided.<sup>44</sup> The dried GO powder was quickly inserted into a muffle furnace preheated to 1050 °C and held in the furnace for 30 s to form reduced graphene oxide (RGO). The yield of RGO relative to the starting amount of GO was ~35%.

### **Fabrication of TPU/RGO nanocomposites**

A series of TPU nanocomposites containing 0, 0.3, 0.5, 1.1, 1.6, 2.7 and 5.5 vol. % RGO were prepared by solution blending technique followed by compression molding. The TPU nanocomposite samples were designated as PUG x where 'x' stands for vol. % of RGO in TPU matrix. The densities of TPU and RGO are taken as 1.2 and 2.28 g/cm<sup>3</sup> respectively. TPU granules were dissolved in DMF using magnetic stirring for 4h and RGO powder was uniformly dispersed in DMF in another beaker for 4h by ultrasonication. RGO dispersion in DMF was

added to the polymer solution and thoroughly mixed using a magnetic stirrer for 6h. The resultant solution was then poured in a petridish (diameter 13.5 cm) and placed in a vacuum oven at 80 °C for 12 h. The films were then used to prepare samples of desired thickness by compression moulding at 150 °C.

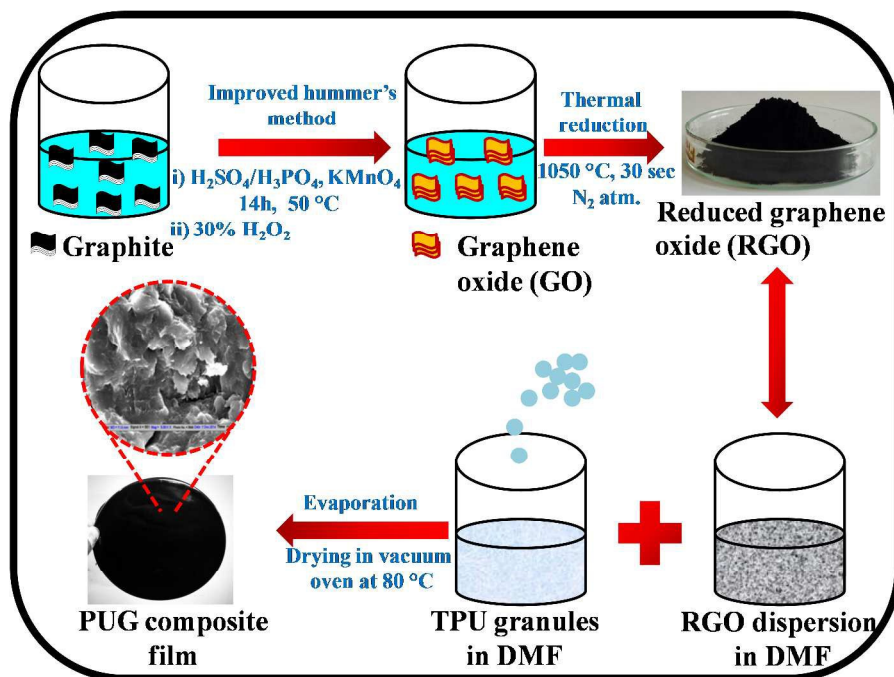


**Fig. 1 Schematic representation of the fabrication process of polyurethane graphene nanocomposite films**

### Characterization

Morphological properties of GO, RGO and PUG nanocomposites were imaged by using a scanning electron microscope (SEM, Zeiss EVO-50) operated at 1kV. Nanocomposite films were broken in liquid nitrogen to obtain cryogenically fractured surfaces and coated with gold in order to limit the charging effects under investigation. High resolution transmission electron microscopy (HRTEM), operating at an accelerating voltage of 300kV and having a point resolution of 0.2 nm, was carried out using a Tecnai G2 F20, USA. The DI Multi-Mode Scanning Probe Microscopy (SMP) with the tapping mode Atomic Force Microscopy (AFM)

technique was used to examine the topography of RGO (Fig. S2 Electronic Supplementary Information (ESI)). The sample for AFM observations was prepared by depositing dispersion of RGO in DMF on a silicon substrate and allowing them to dry in air. The surface area of reduced graphene oxide was measured by using surface area analyzer (Quantachrome® ASiQwin) and quantified by Brunauer-Emmett-Teller (BET) method (see Fig. S1, ESI). Raman spectra were recorded using a Renishaw in Via reflex Raman spectrometer, UK, with an excitation source of 785 nm. The electrical conductivity of the composite films were measured by d.c. four probe contact method using a Keithley 224 programmable current source for providing current. The voltage drop was measured by Keithley 197A auto ranging digital microvolt meter. The values reported in text are averaged of at least five readings of voltage drop at different positions on the sample. Antistatic properties were examined by charge decay measurements after corona charging, using JCI 155 v5 apparatus produced by John Chubb Instrumentation, UK. Charge decay test unit is operated under software control. Positive and negative corona voltage 5 kV was applied to the test samples at room temperature. The software provided opportunity to measure average initial voltage developed by the charge deposited and to record the charge decay curves. The room temperature EMI shielding properties of the PUG nanocomposites were measured by recording the scattering parameters on a vector network analyzer (VNA E8263B Agilent Technologies) in the frequency range of 8.2-12.4 GHz (X band) using a two port measurement technique. The measured scattering parameters were  $S_{11}$  (the forward reflection co-efficient),  $S_{21}$  (the forward transmission coefficient),  $S_{12}$  (the reverse transmission co-efficient) and  $S_{22}$  (the reverse reflection co-efficient). The unit for S parameters is decibel (dB). The VNA was calibrated prior to each measurement sequence to minimize the error. The compression molded

rectangular pellets with dimensions  $22.8 \times 10\text{mm}^2$  of thickness 3mm were inserted in a sample holder connected between the waveguide flanges of a network analyzer.

## Results and discussion

### Morphological and structural aspects of GO and RGO

To investigate the morphology and structure of GO and RGO, scanning and transmission electron microscopy and Raman spectroscopy were recorded for GO and RGO. SEM images revealed the thick carpet like morphology of GO as shown in Fig. 2a. The SEM micrograph of GO after reduction i.e. RGO (Fig. 2b) shows randomly aggregated, thin, characteristic crumpled texture of few layered graphene sheets associated with each other and forming a disordered solid.<sup>45</sup> The TEM image of GO (Fig. 2c) clearly show the transparent film microstructure with folds. TEM micrograph of RGO (Fig. 2d) clearly depicts a large, ultrathin and transparent silk curtain wave like structure with large number of wrinkles on the surface.

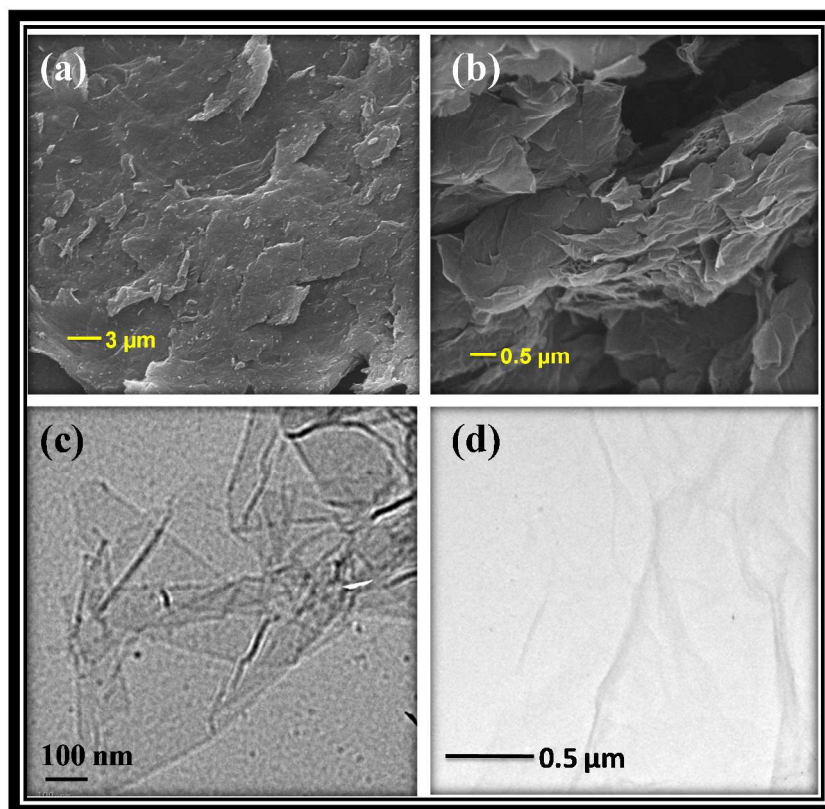


**Fig. 2 SEM and TEM micrographs of GO (a and c) and RGO (b and d)**

Beyond the typical SEM and TEM measurements, a further structural change was investigated using Raman spectroscopy, (Fig. 3). There are two important characteristic Raman bands in graphite like materials: the defect induced disordered band (D-band) that appears between 1300 and 1400  $\text{cm}^{-1}$ , and tangential modes (G-band) that lie in the range from  $\sim 1560$  to  $\sim 1600$   $\text{cm}^{-1}$ .<sup>46</sup> The D-band is present in all graphite-like carbons and originates from structural defects. Therefore, the intensity ratio of D/G modes is conventionally used to quantify the structural quality of graphitic materials. The G-band corresponds to planar vibrations of carbon atoms and is present in most graphite like materials (at around 1580  $\text{cm}^{-1}$ ). The 2D band is the secondary D band caused by the two phonon lattice vibrational process and is an efficient way to estimate the number of layers in graphitic materials.<sup>47</sup> The Raman spectrum of graphite powder, as expected, displays D, G and 2D-band at 1352, 1581 and 2722  $\text{cm}^{-1}$ , respectively on excitation at 514nm. GO also presented characteristic D and G peaks at 1352 and 1592  $\text{cm}^{-1}$ , respectively with an  $I_D/I_G$  ratio of 0.96 (which is greater than 0.28 for graphite).

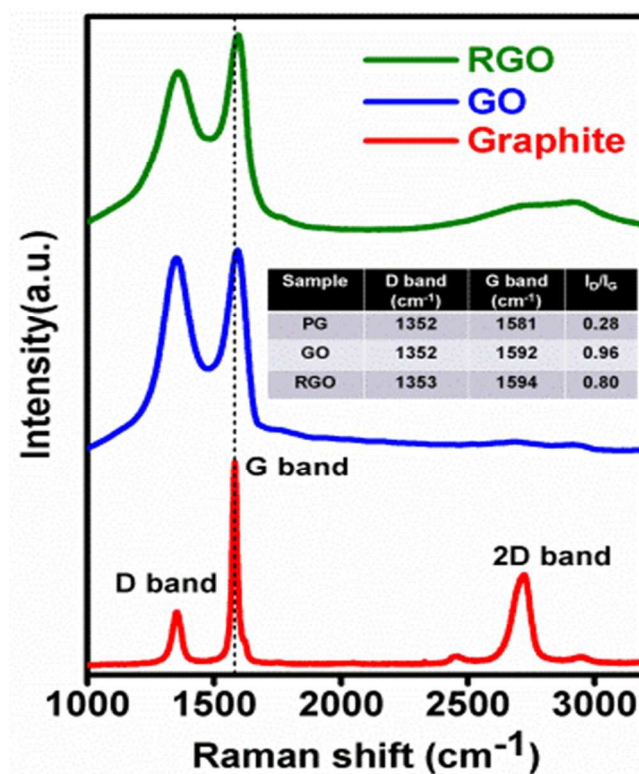


Fig. 3 Raman spectra of GO and RGO

As can be seen in the figure, the FWHM of both the peaks in GO has broadened due to disorder induced by the extensive oxidation of  $sp^2$  domains leading to the reduction in size of the in-plane  $sp^2$  domains and hence the structural imperfections created by the attachment of myriad oxygen functionalities on the basal plane of carbon. The Raman spectrum of RGO also contains well documented both D and G bands (at 1353 and 1594  $cm^{-1}$ , respectively) with an  $I_D/I_G$  ratio of 0.80.

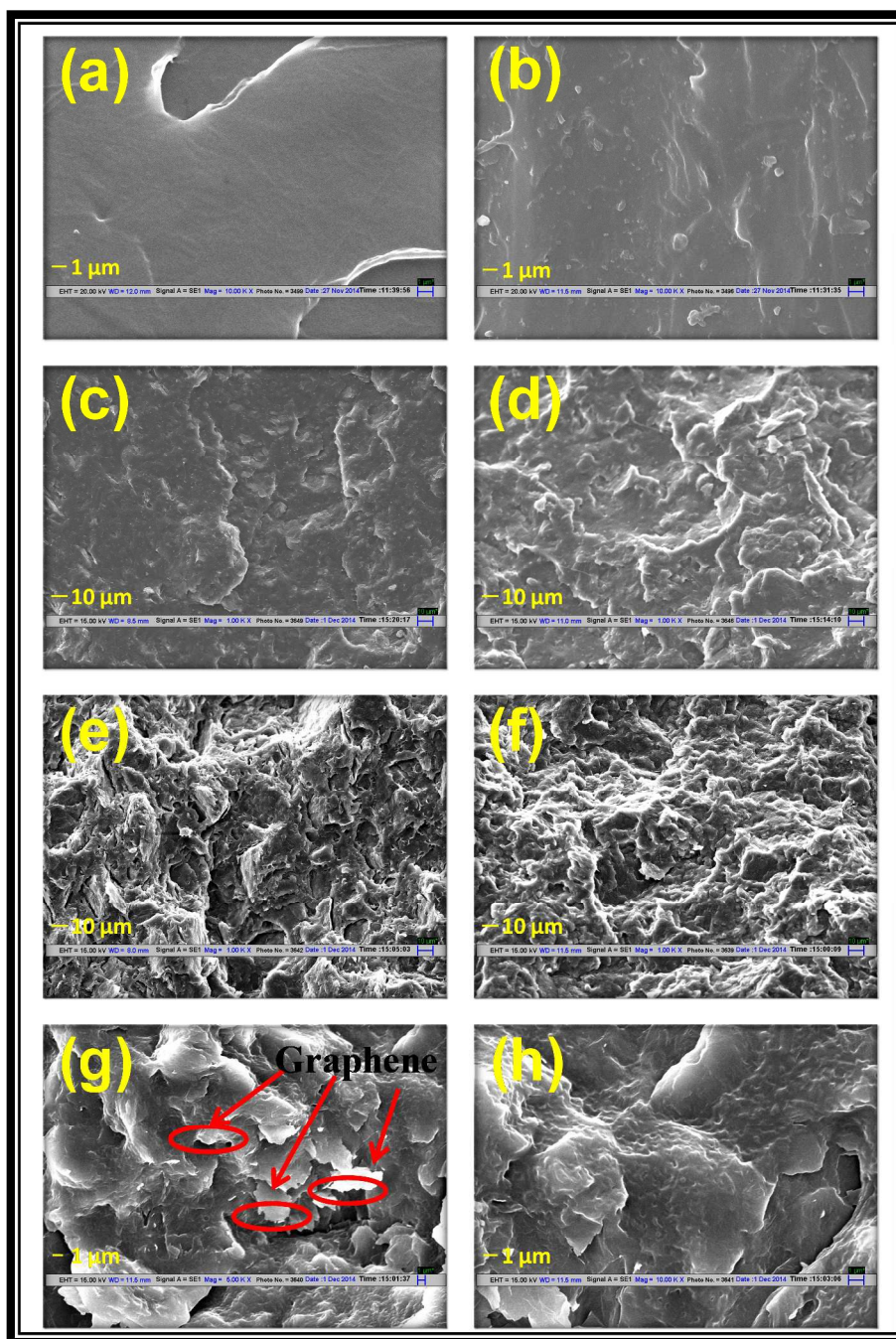
### Morphology observations of PUG composites

Fig. 4 shows a typical overview on the cryofracture surfaces of pure TPU and nanocomposites with different RGO contents. Fig. 4a shows a continuous morphology, smooth and clean rupture surface caused by the brittle failure of the pure TPU matrix. The fractured surfaces of nanocomposites appear to be rougher like scattered island structures, as shown in Fig. 4b-f. As expected, the solution blending technique resulted in relatively good dispersion of RGO

nanosheets in TPU matrix. The polymer shows uniform adherence with the filler nanosheets and this adhesion is indicative of strong interactions between filler and matrix. Uniform distribution of randomly oriented graphene layers reveals the formation of conducting pathway at lower loading which is confirmed by the percolation threshold value (0.44 vol. %, discussed in electrical conductivity section).

### **Electrical conductivity**

Fig. 5 depicts the electrical conductivity values of PUG composites measured by four probe method, which is plotted as a function of RGO content. The conductivity of neat TPU ( $3.9 \times 10^{-11}$  S/cm) is consistent with the values reported in the literature.<sup>35</sup> A significant improvement in electrical conductivity was observed with the increase in graphene content. Incorporation of only 0.3 vol % of RGO leads to an upsurge (almost 4 orders of magnitude) in the electrical conductivity value from  $3.9 \times 10^{-11}$  S/cm (for PUG 0) to  $2.4 \times 10^{-7}$  S/cm (for PUG 0.2) indicating the formation of percolating network or a continuous path for electrical conduction. Maximum



**Fig. 4: SEM micrographs of the fractured surfaces of (a) PUG 0, (b) PUG 0.3, (c) PUG 1.1, (d) PUG 1.6, (e) PUG 2.7, (f) PUG 5.5, (g) and (h) PUG 5.5 at high magnification**

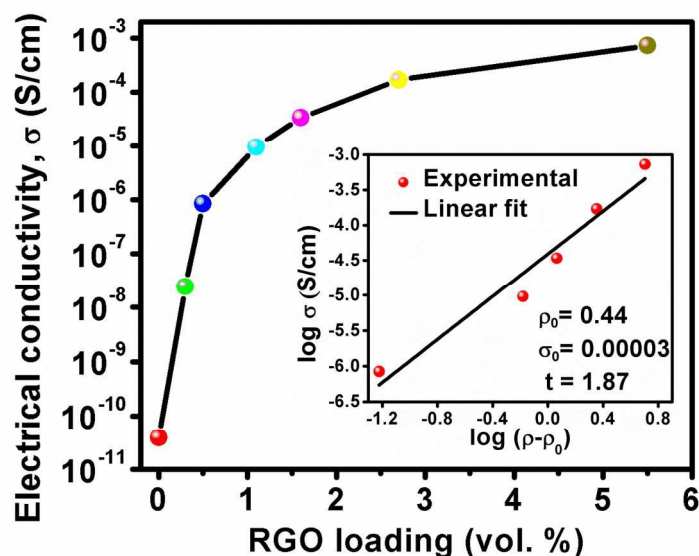


**Fig. 5: Variation in electrical conductivity with RGO loading in TPU matrix. Inset showing  $\log(\sigma)$  vs.  $\log(\rho - \rho_0)$  plot**

electrical conductivity obtained for 5.5 vol. % RGO/PU composite is of order of  $7.3 \times 10^{-4}$  S/cm. The percolation threshold has been predicted by plotting the electrical conductivity as a function of RGO loading and performing data fitting using the scaling law:

$$\sigma = \sigma_0 (\rho - \rho_0)^t \quad (1)$$

where  $\sigma$  is the electrical conductivity of the composite,  $\sigma_0$  is the characteristic conductivity,  $\rho$  is the volume fraction of filler,  $\rho_0$  is the volume fraction at the percolation threshold and  $t$  is the critical exponent related to the system dimensionality.<sup>48</sup> The equation can also be written by taking logarithm of both sides:

$$\log(\sigma) = \log(\sigma_0) + t \log(\rho - \rho_0) \quad (2)$$

By taking the linear regression of  $\log(\sigma)$  vs.  $\log(\rho - \rho_0)$  plot, both percolation threshold and critical exponent can be evaluated. As, percolation threshold is the minimum filler content where first continuous network of filler particles is formed within the polymer matrix, both lower percolation threshold and higher critical exponent are indicative of homogeneous dispersion of

filler within the matrix as described somewhere else.<sup>49</sup> Parameter values obtained from the fitting of electrical conductivity data into the scaling law are:  $\rho_0 = 0.44$  vol. % and  $t = 1.87$ . The  $\log(\sigma)$  vs.  $\log(\rho - \rho_0)$  plot shows a straight line displaying an excellent fit to the data. For the composite material, the percolation threshold was observed at 0.44 vol. % for RGO loading. The value of critical exponent obtained from the fit is in good agreement with estimated value from the percolation theory for a 3D conducting network in an insulating polymer matrix.<sup>48</sup>

### **ESD response of PUG composites**

In order to study the potential of PUG nanocomposites for electronics applications, their ESD and EMI shielding properties were investigated. Generally, electrical conductivities in the range of  $10^{-11} - 10^{-6}$  S/cm suffice for dissipating electrostatic charge.<sup>50</sup> Therefore, for ESD studies low loading PUG composites (up to 1.6 vol. %) were selected whereas high loading were preferred for EMI shielding studies. The characteristics of decay of surface voltage vs. time for PUG composites after the positive and negative polarization are shown in Fig. 6. There are two criteria to assess the ability of a material to dissipate static charge from its surface:<sup>51</sup>

- (i) Criterion 1/e – decay time measured to 1/e (about 37 %) of the accepted surface voltage;
- (ii) Criterion 10% – decay time measured to 10 % of the accepted surface voltage.

A simple acceptance test criterion is that the decay time should be:

- i) Less than half a second in the 1/e criterion;
- ii) Less than 2s in the 10 % criterion.

The solution casted films of PUG composites were used for the measurement of static decay time on Static Decay Meter by measuring the time on applying a corona charging voltage of  $\pm 5.0$  kV and recording the voltage till it is decayed to 1/e and 10 % of the accepted surface voltage. The

results show that the accepted voltage obeys an exponential decay with time marked by an initial sharp decay followed by a plateau region. It was observed that the pure polyurethane film (PUG 0) shows a static decay time of 5.42s and 38.4s at 1/e and 10% cut-off respectively after accepting 729.59 V ( ~14.5 % of the applied voltage (+5.0 kV)). Similarly, the static decay time of 5.71s and 41.77s at 1/e and 10% cut-off respectively was observed for PUG 0 after receiving -968.75 V (~19.3 % of the applied voltage (-5.0 kV)). Based on the above observations, we can say that PUG 0 shows poor antistatic response and longer times are required to dissipate the static charge from its surface. However, on incorporation of RGO in the polyurethane matrix, charge acceptability and retention capability decreases drastically due to rapid charge dissipation. Therefore, when a positive potential of 5.0 kV was applied to PUG 0.3, it accepted only 556.77 V which was rapidly dissipated and reached the 1/e and 10 % cutoff limit within 0.52s and 1.63s respectively, demonstrating that the sample passes the antistatic criteria of 2s. Similarly, other composites also display rapid charge drainage with static decay time of less than 2s, after positive or negative high corona voltage was applied to the surface of the material and ensure efficient antistatic response of materials under service conditions. All the decay time measurement values are shown in the Fig. 6.

The surface voltage received by the material depends on the nature of the materials. When high corona voltage was applied on the surface of the insulating material, only a limited amount of voltage was retained on its surface whereas larger amount of voltages were drained away. However, with the incorporation of electrically conducting filler, the electrical conductivity of the material increases which decreases the charge retention capability by reducing the decay time. Hence, the improved antistatic response of PUG 0.3 – 1.6 composites arises due to the

conducting network formed by the RGO sheets within the polyurethane matrix. Moreover, the received voltage by the samples after negative corona charging was considerably greater than by

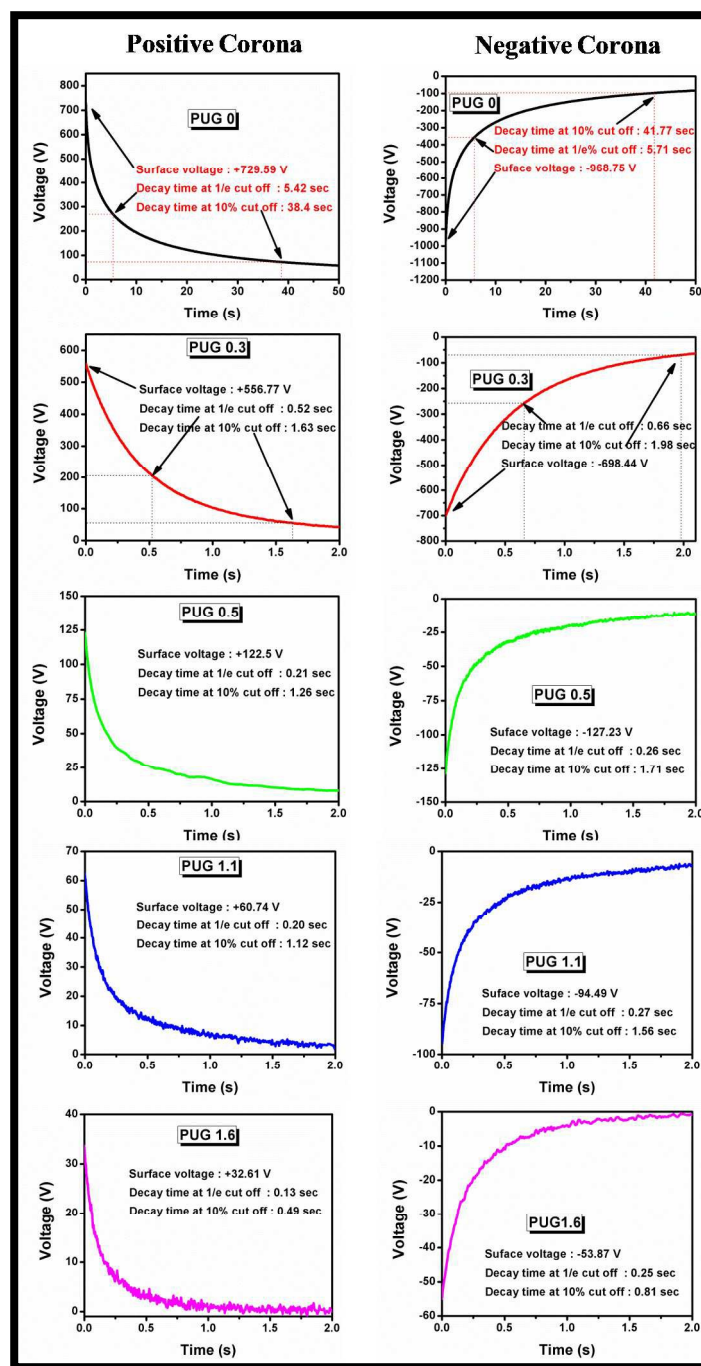


Fig. 6: Electrostatic charge dissipative graphs of PUG nanocomposites showing voltage decay as a function of time

the positive one which may be the reason for the longer decay times for negative corona. The reason of that can be a fact that in a negative corona total number of electrons may be much higher though the number of very high energy electrons may be lower when compared to a positive corona.<sup>50</sup>

The electrical conductivity of PUG samples beyond 1.6 vol. % was in the range which is suitable for efficient EMI shielding effectiveness. Therefore EMI shielding effectiveness of these composites has been studied.

### **EMI shielding performance of PUG composites**

Electromagnetic interference shielding effectiveness (EMI SE) is the ability of a material to attenuate an incident electromagnetic radiation and is defined by the following equation<sup>52-53</sup>,

$$SE = 10 \log (P_t/P_i) = 20 \log (E_t/E_i) = 20 \log (H_t/H_i) \quad (3)$$

where symbols P, E and H stand for power, electric and magnetic field intensity, respectively.

The subscripts 't' and 'i' are used for the transmitted and incident wave on the shield, respectively. EMI shielding consists of three different mechanisms; namely reflection, absorption and multiple-reflection. The EMI shielding effectiveness (SE) of a shielding material is the sum of shielding effectiveness due to reflection ( $SE_R$ ), absorption ( $SE_A$ ), and multiple reflections ( $SE_M$ ).

$$SE = SE_R + SE_A + SE_M \quad (4)$$

The reflection is related to the impedance mismatch between air and absorber; the absorption is resulted from the energy dissipation of EM radiations; and the multiple reflections are induced by the scattering effect of the inhomogeneity in the material.<sup>54</sup> The multiple reflection term ( $SE_M$ ) can be ignored in cases where the contribution of absorption to EMI SE is more than -10 dB or if the shield is thicker than the skin depth.<sup>55</sup> In general, the SE of a shielding material is

commonly expressed in decibels (dB). A higher SE value indicates less energy that is transmitted through the shielding material. Thus, SE can be expressed as,

$$SE \text{ (dB)} = SE_A \text{ (dB)} + SE_R \text{ (dB)} \quad (5)$$

The EMI SE of PUG composite with varying loading of RGO was measured over the frequency range of 8.2-12.4 GHz (Fig 7a). The results revealed that the EMI SE increases with increasing RGO content e.g. PUG 0 displaying poor EMI shielding response (i.e. SE ~ -3dB) whereas SE of -21dB obtained for PUG 5.5 that corresponds to blocking of more than 99% of the incident EM radiations. This improvement can be ascribed to the formation of conducting network throughout the electrically insulating polyurethane matrix. This value is in the limits of the target value (~ -20 dB) of EMI SE required for the techno-commercial applications. The mechanism of EMI shielding was analyzed by plotting SE,  $SE_A$  and  $SE_R$  of PUG composites as a function of RGO loading at mid frequency of 10.3 GHz. For the PUG 5.5 composite, the value of SE,  $SE_A$  and  $SE_R$  are -20.9, -17.6, and -3.3 dB respectively. The fig (7b) shows that though both  $SE_A$  and  $SE_R$  increase with RGO loading,  $SE_A$  increases more rapidly compared to the corresponding  $SE_R$  component. This behavior can be attributed to the EMI shielding mechanism being dominated by absorption and a similar growth trend in SE was also seen.

An incident electromagnetic wave penetrating through the shield decays inside it by conductive dissipation.<sup>38</sup> High electrical conductivity and the formation of conductive networks within the matrix play an important role in the EMI shielding performance of the composites. The residual defects present in RGO are helpful in impedance matching, defect polarization relaxation and electronic dipole relaxation, which all serve to improve electromagnetic wave absorption.<sup>23</sup> Also, the large surface and interface areas of RGO in the composite increase the probability of more interaction with the incident EM wave.

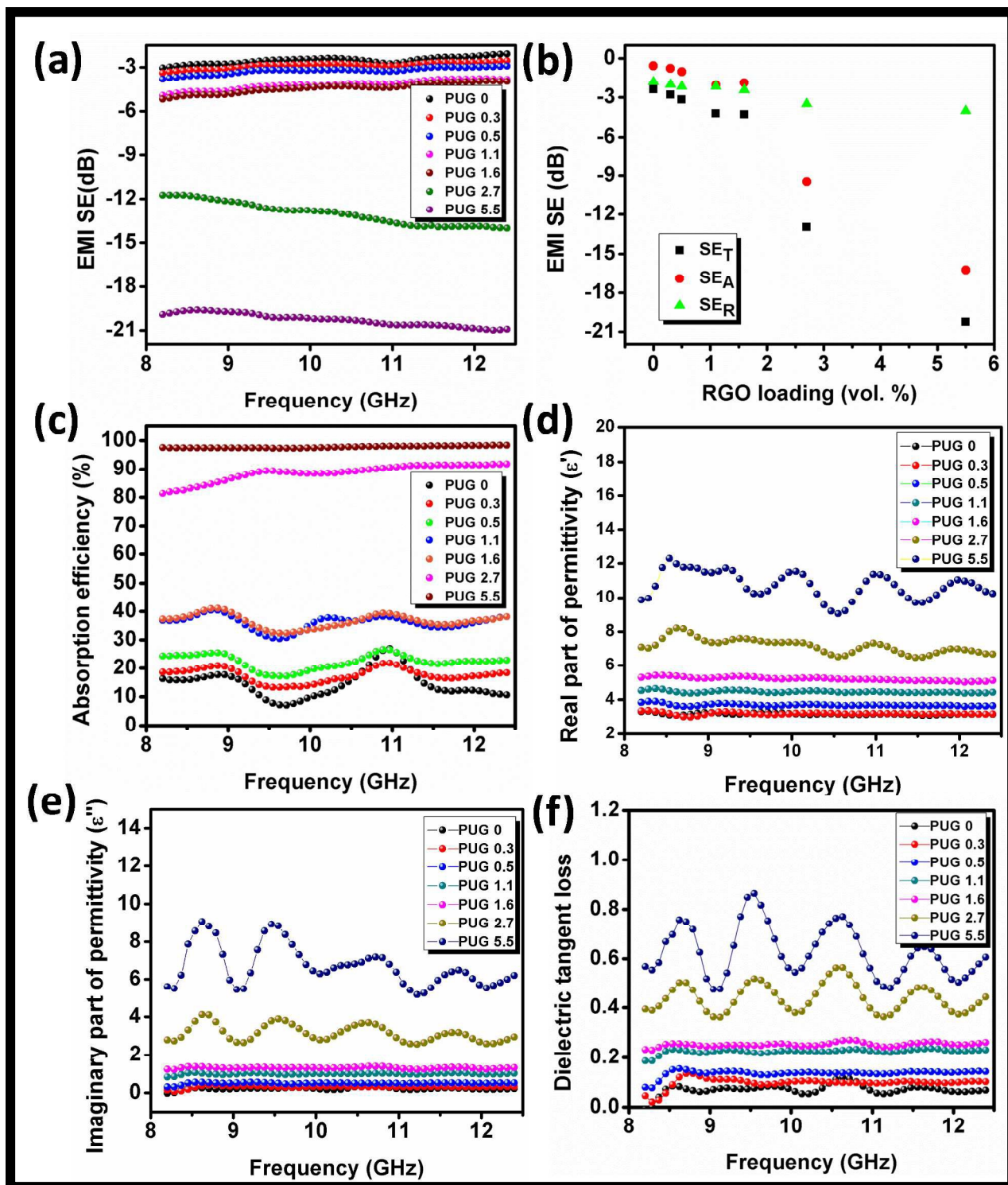


Fig. 7: (a) Variation in EMI shielding effectiveness with frequency for PUG nanocomposites, (b) Variation in SE<sub>T</sub>, SE<sub>A</sub> and SE<sub>R</sub> with RGO loading at 10.5 GHz, (c) variation in absorption efficiency, frequency dependence of (d) real and (e) imaginary parts of permittivity and dielectric loss tangent for PUG nanocomposites

Therefore it is difficult for the incident EM wave to escape from the PUG composite. These EM waves are absorbed and transformed into thermal energy by the continuous RGO networks. The developed PUG 5.5 composite exhibited an absorption efficiency of more than 98 % (Fig. 7c), which means most of the EM energy incident on the shield attenuates and dissipates in the form of heat energy.<sup>56</sup>

To elaborate more about the shielding performance of PUG composites, electromagnetic attributes such as complex permittivity of the composites was explored using the S parameters. The real part of the complex permittivity is mainly associated with the amount of polarization occurring in the material and symbolizes the storage ability of the electrical energy (also known as dielectric constant), whereas the imaginary part accounts for the dielectric losses.<sup>8</sup> The frequency dependence of the real and imaginary part of permittivity for PUG composites are shown in Fig. 7d and 7e. The results show that with the increase in the RGO loading level, the real part of permittivity varies from 3.3 to 12.6 whereas the imaginary part of permittivity varies from 0.1 to 8.6 for the PUG composites. It is proposed that the increase in the dielectric properties is a direct consequence of the increased electrical conductivity and electric polarization in the PUG composites because the relative complex permittivity, which is a measure of the polarizability of a material, induces dipolar and electric polarization during activation by an EM wave.<sup>23</sup> The ratio of the imaginary to the real part is the ‘dissipation factor’, which is represented by  $\tan \delta$ , where  $\delta$  is called “loss angle”, denoting the angle between the voltage and the charging current. Fig. 7f shows the plots of  $\tan \delta$  vs. frequency of PUG nanocomposites as a function of RGO loading. Since,  $\tan \delta$  value indicates the absorptive property of a material, i.e., the ability of a material to convert applied energy into heat; materials

with high  $\tan \delta$  value are used as microwave absorbing materials and in stealth technology.<sup>57</sup> The  $\tan \delta$  values of PUG composites increased with increasing RGO content and  $\tan \delta$  value of 0.65 – 0.7 was observed for PUG 10 composite. It is proposed that the humps observed in the dielectric properties (at higher loading of RGO) are suggestive of two main phenomena responsible for dielectric losses. These are due to interfacial polarization between RGO sheets in the matrix and high anisotropy energy of the nanocomposites.<sup>24</sup> Thus, it is concluded that the EMI SE of PUG composites depends on RGO loading and the EMI SE is strongly related to electrical conductivity and dielectric properties of the material. From all the above mentioned discussion, it is concluded that the polyurethane filled graphene composites may be used as electrostatic discharge protection at low graphene loading and effective candidates for EMI shielding in the X-band of microwave frequency range at higher graphene loading.

### **Conclusion**

This paper presented the designing of graphene filled thermoplastic polyurethane nanocomposites for two applications: ESD and EMI shielding on the basis of tailoring the electrical conductivity as a consequence of graphene loading. These composites show a low percolation threshold of 0.44 vol. % which is mainly attributed to the formation of first continuous network of conducting interconnected graphene nanosheets in the insulating polyurethane matrix. The developed PUG nanocomposite exhibited an EMI shielding value of -21dB in the X-band of frequency range for 5.5 vol. % loading indicating that the composites can meet the commercial application demands. In addition, a quantitative measurement of electrostatic dissipative properties of graphene filled polyurethane was also presented speculating the use of such PUG nanocomposites for ESD applications. These results, combined with the advantages of a cheap and abundant supply of graphite and the solution processability of

graphene sheets, indicate that such nanocomposites can be used as effective and lightweight shielding materials against electromagnetic pollution and electrostatic dissipation.

### Acknowledgement

The authors thank the Ministry of Human Resource Development (MHRD), India for providing financial assistance to one of the authors Mrs. Meenakshi Verma and IIT Delhi for providing all the facilities.

### References

1. D. D. L. Chung, *Carbon*, 2001, **39**, 279-285.
2. A. P. Singh, M. Mishra, P. Sambyal, B. K. Gupta, B. P. Singh, A. Chandra and S. K. Dhawan, *Journal of Materials Chemistry A*, 2014, **2**, 3581-3593.
3. S. He, G.-S. Wang, C. Lu, J. Liu, B. Wen, H. Liu, L. Guo and M.-S. Cao, *Journal of Materials Chemistry A*, 2013, **1**, 4685-4692.
4. X.-J. Zhang, G.-S. Wang, W.-Q. Cao, Y.-Z. Wei, J.-F. Liang, L. Guo and M.-S. Cao, *ACS Applied Materials & Interfaces*, 2014, **6**, 7471-7478.
5. S. D. Ramôa, G. M. Barra, R. V. Oliveira, M. G. de Oliveira, M. Cossa and B. G. Soares, *Polymer International*, 2013, **62**, 1477-1484.
6. Z. Chen, C. Xu, C. Ma, W. Ren and H.-M. Cheng, *Advanced Materials*, 2013, **25**, 1296-1300.
7. N. Yousefi, X. Sun, X. Lin, X. Shen, J. Jia, B. Zhang, B. Tang, M. Chan and J. K. Kim, *Advanced Materials*, 2014, **26**, 5480-5487.
8. K. Singh, A. Ohlan, V. H. Pham, B. R. S. Varshney, J. Jang, S. H. Hur, W. M. Choi, M. Kumar, S. K. Dhawan, B.-S. Kong and J. S. Chung, *Nanoscale*, 2013, **5**, 2411-2420.
9. Y. L. F. Musico, C. M. Santos, M. L. P. Dalida and D. F. Rodrigues, *Journal of Materials Chemistry A*, 2013, **1**, 3789-3796.
10. M. Sun, G. Wang, C. Yang, H. Jiang and C. Li, *Journal of Materials Chemistry A*, 2015, **3**, 3880-3890.
11. H. Wang, Q. Hao, X. Yang, L. Lu and X. Wang, *Nanoscale*, 2010, **2**, 2164-2170.
12. B. G. Choi, M. Yang, W. H. Hong, J. W. Choi and Y. S. Huh, *ACS Nano*, 2012, **6**, 4020-4028.
13. C. Berger, Z. Song, T. Li, X. Li, A. Y. Ogbazghi, R. Feng, Z. Dai, A. N. Marchenkov, E. H. Conrad, P. N. First and W. A. de Heer, *The Journal of Physical Chemistry B*, 2004, **108**, 19912-19916.
14. P. Bhattacharya, S. Dhibar, G. Hatui, A. Mandal, T. Das and C. K. Das, *RSC Advances*, 2014, **4**, 17039-17053.
15. J. Shen, K. Han, E. J. Martin, Y. Y. Wu, M. C. Kung, C. M. Hayner, K. R. Shull and H. H. Kung, *Journal of Materials Chemistry A*, 2014, **2**, 18204-18207.

16. F. Zhang, T. Zhang, X. Yang, L. Zhang, K. Leng, Y. Huang and Y. Chen, *Energy & Environmental Science*, 2013, **6**, 1623-1632.
17. G. Diao, S. Zhu, M. Chen, W. Ren, J. Yang, S. Qu and Z. Li, *New Journal of Chemistry*, 2015.
18. Y. Dong, Z. Zhang, Y. Xia, Y.-S. Chui, J.-M. Lee and J. A. Zapien, *Journal of Materials Chemistry A*, 2015, **3**, 16206-16212.
19. C. Perumal Veeramalai, F. Li, H. Xu, T. W. Kim and T. Guo, *RSC Advances*, 2015, **5**, 57666-57670.
20. B. Wang, G. Wang and H. Wang, *Journal of Materials Chemistry A*, 2015.
21. Y. Zhang, L. Jiang and C. Wang, *Physical Chemistry Chemical Physics*, 2015, **17**, 20061-20065.
22. C. L. Weaver, H. Li, X. Luo and X. T. Cui, *Journal of Materials Chemistry B*, 2014, **2**, 5209-5219.
23. M. Verma, A. P. Singh, P. Sambyal, B. P. Singh, S. K. Dhawan and V. Choudhary, *Physical Chemistry Chemical Physics*, 2015, **17**, 1610-1618.
24. N. Yousefi, X. Sun, X. Lin, X. Shen, J. Jia, B. Zhang, B. Tang, M. Chan and J.-K. Kim, *Advanced Materials*, 2014, **26**, 5480-5487.
25. D.-X. Yan, P.-G. Ren, H. Pang, Q. Fu, M.-B. Yang and Z.-M. Li, *Journal of Materials Chemistry*, 2012, **22**, 18772-18774.
26. T. T. Tung, J.-F. Feller, T. Kim, H. Kim, W. S. Yang and K. S. Suh, *Journal of Polymer Science Part A: Polymer Chemistry*, 2012, **50**, 927-935.
27. X. Sun, J. He, G. Li, J. Tang, T. Wang, Y. Guo and H. Xue, *Journal of Materials Chemistry C*, 2013, **1**, 765-777.
28. S. Husić, I. Javni and Z. S. Petrović, *Composites Science and Technology*, 2005, **65**, 19-25.
29. S. Ummartyotin, J. Juntaro, M. Sain and H. Manuspiya, *Industrial Crops and Products*, 2012, **35**, 92-97.
30. S. Mondal and J. Hu, *Indian Journal of Fibre and Textile Research*, 2006, **31**, 66.
31. M. C. Ifeyinwa and U. Reginald, *Europe*, **3**, 5.
32. U. Meier-Westhues, *Polyurethanes: coatings, adhesives and sealants*, Vincentz Network GmbH & Co KG, 2007.
33. T. K. Gupta, B. P. Singh, S. R. Dhakate, V. N. Singh and R. B. Mathur, *Journal of Materials Chemistry A*, 2013, **1**, 9138-9149.
34. T. K. Gupta, B. P. Singh, S. Teotia, V. Katyal, S. R. Dhakate and R. B. Mathur, *Journal of Polymer Research*, 2013, **20**, 1-7.
35. J. Bian, H. L. Lin, F. X. He, X. W. Wei, I. T. Chang and E. Sancaktar, *Composites Part A: Applied Science and Manufacturing*, 2013, **47**, 72-82.
36. M. Valentini, F. Piana, J. Pionteck, F. R. Lamastra and F. Nanni, *Composites Science and Technology*, 2015, **114**, 26-33.
37. L. Yang, S. L. Phua, C. L. Toh, L. Zhang, H. Ling, M. Chang, D. Zhou, Y. Dong and X. Lu, *RSC Advances*, 2013, **3**, 6377-6385.
38. S.-T. Hsiao, C.-C. M. Ma, W.-H. Liao, Y.-S. Wang, S.-M. Li, Y.-C. Huang, R.-B. Yang and W.-F. Liang, *ACS Applied Materials & Interfaces*, 2014, **6**, 10667-10678.
39. S.-T. Hsiao, C.-C. M. Ma, H.-W. Tien, W.-H. Liao, Y.-S. Wang, S.-M. Li and Y.-C. Huang, *Carbon*, 2013, **60**, 57-66.

40. S.-T. Hsiao, C.-C. M. Ma, H.-W. Tien, W.-H. Liao, Y.-S. Wang, S.-M. Li, C.-Y. Yang, S.-C. Lin and R.-B. Yang, *ACS Applied Materials & Interfaces*, 2015, **7**, 2817-2826.
41. L. He and S. C. Tjong, *RSC Advances*, 2015, **5**, 15070-15076.
42. C. Liu, H. Yan, L. Yuan, Z. Chen and M. Zhang, *Journal of Polymer Science Part A: Polymer Chemistry*, 2015, n/a-n/a.
43. H. Wang, G. Xie, M. Fang, Z. Ying, Y. Tong and Y. Zeng, *Composites Part B: Engineering*, 2015, **79**, 444-450.
44. D. C. Marcano, D. V. Kosynkin, J. M. Berlin, A. Sinitskii, Z. Sun, A. Slesarev, L. B. Alemany, W. Lu and J. M. Tour, *ACS Nano*, 2010, **4**, 4806-4814.
45. T. K. Gupta, B. P. Singh, R. K. Tripathi, S. R. Dhakate, V. N. Singh, O. Panwar and R. B. Mathur, *RSC Advances*, 2015, **5**, 16921-16930.
46. H. Zhang, D. Hines and D. L. Akins, *Dalton Transactions*, 2014, **43**, 2670-2675.
47. A. Metin and L. A. Daniel, 2013.
48. A. Aharony and D. Stauffer, *Introduction to percolation theory*, Taylor & Francis, 2003.
49. M. Weber and M. R. Kamal, *Polymer composites*, 1997, **18**, 711-725.
50. H. Bhandari, S. Singh, V. Choudhary and S. K. Dhawan, *Polymers for Advanced Technologies*, 2011, **22**, 1319-1328.
51. B. Gornicka, M. Mazur, K. Sieradzka, E. Prociow and M. Lapinski, *Acta Physica Polonica-Series A General Physics*, 2010, **117**, 869.
52. N. Das, D. Khastgir, T. Chaki and A. Chakraborty, *Composites Part A: Applied Science and Manufacturing*, 2000, **31**, 1069-1081.
53. P. Saini, V. Choudhary, B. P. Singh, R. B. Mathur and S. K. Dhawan, *Materials Chemistry and Physics*, 2009, **113**, 919-926.
54. W. Chen, J. Wang, T. Wang, J. Wang and B. Zhang, *Journal of Reinforced Plastics and Composites*, 2015, 0731684415586610.
55. B. Singh, K. Saini, V. Choudhary, S. Teotia, S. Pande, P. Saini and R. Mathur, *Journal of Nanoparticle Research*, 2014, **16**, 1-11.
56. S. Maiti, N. K. Shrivastava, S. Suin and B. B. Khatua, *ACS Applied Materials & Interfaces*, 2013, **5**, 4712-4724.
57. A. Gupta and V. Choudhary, *Composites Science and Technology*, 2011, **71**, 1563-1568.